An Inorganic Double Helix Sheathing Alkali Metal Cations: $ANb_2P_2S_{12}$ (A = K, Rb, Cs), A Series of Thiophosphates Close to the Metal–Nonmetal Boundary—Chalcogenide Analogues of Transition-Metal Phosphate Bronzes?

Christine Gieck,[a] Volkmar Derstroff,[a] Thomas Block,[a] Claudia Felser,[a] Guido Regelsky,[c] Ove Jepsen,[b] Vadim Ksenofontov,[a] Philipp Gütlich,[a] Hellmut Eckert,*[c] and Wolfgang Tremel*[a]

Dedicated to Professor Bernt Krebs on the occasion of his 65th birthday

Abstract: The new quaternary niobium thiophosphates $ANb_2P_2S_{12}$ (A = K, Rb, Cs) have been prepared and characterized. The title compounds were synthesized by reacting Nb metal, A_2S, P_2S_5, and S at 600–700 °C in evacuated silica tubes. They crystallize as "stuffed" variants of the tetragonal $TaPS_6$ structure type in the tetragonal space group $I\bar{4}2d$ with eight formula units per unit cell and lattice constants $a = 15.923(2)$ and $c = 13.238(3)$ Å for $CsNb_2P_2S_{12}$, $a = 15.887(3)$ and $c = 13.132(3)$ Å for $RbNb_2P_2S_{12}$, and $a = 15.850(2)$ and $c = 13.119(3)$ Å for $KNb_2P_2S_{12}$. Their structures are based on double helices formed from interpenetrating, noninteracting spiral chains of binuclear $[Nb_2S_{12}]$ cluster units and $[PS_4]$ thiophosphate groups. The cavities and tunnels, which are formed by the helical chains, are filled with A^+ ions. Temperature-dependent conductivity studies reveal thermally activated electrical transport behavior. This result is consistent with the observation of a temperature-dependent contribution to the ^{31}P MAS-NMR shift, suggesting that the delocalized s-electron spin density increases with increasing temperature. These findings are supported by the results of tight-binding band structure calculations which reveal that the unusual electrical transport behavior of $ANb_2P_2S_{12}$ is a consequence of the structure symmetry. Therefore, $CsNb_2P_2S_{12}$ may be considered a chalcogenide analogue of metal phosphate bronzes.

Keywords: chalcogenides · electronic structure · niobium · phosphates · solid-state structures

Introduction

Early transition-metal bronzes with the general formulae $A_xM_yO_z$ (M = Ti, Nb, Mo, W)[1] and $(PO_2)_4(MO_3)_{2m}$[2] have furnished a seemingly endless number of electronic surprises. The continuing interest in the reduced metal oxides has been nourished by the discovery of charge-density wave (CDW) phenomena in the molybdenum bronzes.[3] The discovery of multiple CDWs in the 2D monophosphate tungsten bronzes $(PO_2)_4(WO_3)_{2m}$[2] and superconductivity in several tungsten bronzes[4] provided further impetus to the field. A group of low-dimensional compounds with comparable properties are early transition-metal chalcogenides such as MQ_2 (Q = S, Se),[5] A_XMQ_2 (M = Ti, Nb, Ta; Q = S, Se),[6] $NbSe_3$[7] or MTe_3 (M = Zr, Hf, Th).[8] It is well known that many of these low-dimensional metals may exhibit two competing types of electronic instabilities: i) the Peierls instability leading to a charge density wave state as observed in transition-metal bronzes or layered transition-metal chalcogenides[1,5,6] or ii) superconductivity as in the high-T_C cuprates.[9] The mechanisms that control the type of instability that is actually observed are not well understood at present. Therefore, one primary goal of preparative solid-state science is the design of new families of low-dimensional conductors with new and unusual structural properties to test—and possibly improve—existing theories of electronic structure.

[a] C. Gieck, Dr. V. Derstroff, T. Block, Dr. C. Felser, Dr. V. Ksenofontov, Prof. Dr. P. Gütlich, Prof. Dr. W. Tremel
Institut für Anorganische Chemie und Analytische Chemie der Johannes Gutenberg-Universität
Duesbergweg 10-14, 55099 Mainz (Germany)
E-mail: tremel@mail.uni-mainz.de

[b] Dr. O. Jepsen
Max Planck-Insitut für Festkörperforschung
Heisenbergstrasse 1, 70569 Stuttgart (Germany)

[c] Dr. G. Regelsky, Prof. Dr. H. Eckert
Institut für Physikalische Chemie der Westfälischen Wilhelms-Universität
Schlossplatz 8, 48149 Münster (Germany)
Fax: (+49) 251-833-3169
E-mail: eckerth@uni-muenster.de

DOI: 10.1002/chem.200103504

From a chemical perspective, it would be attractive to study chalcogenide bronzes, a family of hybrid materials, which combine the properties of both metal bronzes and layered chalcogenides. Surprisingly, however, no chalcogen analogues of the phosphate bronzes are known. A wealth of phases in the M-X-Q families (M = early transition metal, X = Si, Ge, Sn, P, As, Bi; Q = S, Se, Te) have been synthesized during the past decade;[10] their large number originates from the numerous oxidation states that can be taken not only by the transition metal, but also by the main group components. All materials of this family are nonmetallic.

Cation intercalation into a given host structure provides a convenient strategy for the designed synthesis of metallic materials from nonmetallic hosts.[11] Owing to their low-dimensional structures, thiophosphates such as MPQ_3[10] are susceptible to topotactic reactions. Still, the magnetic and semiconducting properties of the resulting materials indicate that synthetic attempts must focus on compounds containing 4d and 5d metals, because the small overlap between the contracted 3d orbitals of the first-row transition metals generally leads to narrow bands and consequently electron localization. A potential host for intercalation reactions among chalcogenides of the heavy transition elements is $TaPS_6$.[12] It crystallizes in a three-dimensional framework structure, whose tunnels have diameters of approximately 5 Å and may trap polymeric sulfur or selenium chains in solid-state reactions or from the gas phase as in $Ta_4P_4S_{29} = (TaPS_6)_4(S_5)$[13] or $TaPS_6(Se)$.[14] Whereas topotactic reactions have not led to the desired products so far, metal-intercalated variants were obtained from high-temperature reactions and topotactic ion exchange. Here we report a structural study of $ANb_2P_2S_{12}$ (A = Cs, Rb, K) and discuss their physical properties with respect to their electronic structure.

Abstract in German: *Die neuartigen Niobthiophosphate $ANb_2P_2S_{12}$ (A = K, Rb, Cs) wurden durch Erhitzen von elementarem Niob, A_2S, Schwefel und P_2S_5 auf 600–700 °C in evakuierten Quarzglasampullen dargestellt. Die Titelverbindungen kristallisieren als aufgefüllte Varianten der tetragonalen $TaPS_6$-Struktur in der Raumgruppe I-42*d *mit acht Formeleinheiten in der Elementarzelle und den Gitterparametern* a = *15.923(2) und* c = *23.238(3) Å für $CsNb_2P_2S_{12}$,* a = *15.887(3) und* c = *13.132(3) Å für $RbNb_2P_2S_{12}$, sowie* a = *15.850(2) und* c = *13.119(3) Å für $KNb_2P_2S_{12}$. Die Gerüststrukturen der Verbindungen enthalten Doppelhelices aus einander durchdringenden spiralartigen Ketten aus $[Nb_2S_{12}]$ Clusterbausteinen und $[PS_4]$-Thiophosphatgruppen. Die Kationen sind in die Kanäle des Strukturgerüsts eingebaut. Die A^+-Kationen in den Zentren der weiten Kanäle sind in allen Verbindungen $ANb_2P_2S_{12}$ (A = K, Rb, Cs) fehlgeordnet über zwei Positionen. Der große Durchmesser der Ionenkanäle sowie die hohen thermischen Parameter der A^+-Kationen deuten an, daß $ANb_2P_2S_{12}$ (A = K, Rb) potentielle Wirtsverbindungen für topotaktische Ionenaustausch-Reaktionen sind. Die Ergebnisse temperaturabhängiger Widerstandsunter-suchungen, magnetischer Suszeptibilitätsmessungen, ^{31}P-MAS-NMR- sowie ESR-spektroskopischer Untersuchungen zeigen, daß $CsNb_2P_2S_{12}$ thermisch-aktivierte Leitfähigkeit aufweist. Diese Befunde werden durch die Ergebnisse von Bandstrukturrechnungen im Rahmen des Tight-Binding-Modells gestützt. Die ungewöhnlichen elektrischen Transporteigenschaften sind durch die Symmetrie der Struktur bedingt. $CsNb_2P_2S_{12}$ ließe sich daher als chalcogenanaloge Phosphatbronze auffassen.*

Results and Discussion

Synthesis: Single-phase $ANb_2P_2S_{12}$ was obtained according to Equation (1) by heating Nb metal with alkali sulfide (A_2S), phosphorus sulfide and sulfur in sealed quartz ampoules for seven days at 600–700 °C in the appropriate stoichiometric ratio followed by cooling to room temperature at a rate of 2 °C h^{-1}.

$$A_2S + 2P_2S_5 + 2Nb + 13S \rightarrow 2ANb_2P_2S_{12} \quad (1)$$

Crystal structure: All compounds of composition $ANb_2P_2S_{12}$ are isostructural. Data for the structures of $ANb_2P_2S_{12}$ are given in Tables 1–3 in the Experimental Section.. A view of the structure along the *c* direction is given in Figure 1. The crystal structures may be considered a stuffed $TaPS_6$ type.[12] The dominating motifs are $[Nb_2S_{12}]$ units and $[PS_4]$ thiophosphate groups where the S atoms of the $[PS_4]$ tetrahedra are the capping and edge sulfur atoms of two adjacent $[Nb_2S_{12}]$ units. The $[Nb_2S_{12}]$ units of $CsNb_2P_2S_{12}$ are composed of distorted bicapped trigonal $[NbS_8]$ prisms sharing a rectangular face to form a $[Nb_2S_{12}]$ biprism with an average Nb–S bond length of 2.549 Å (with individual dis-

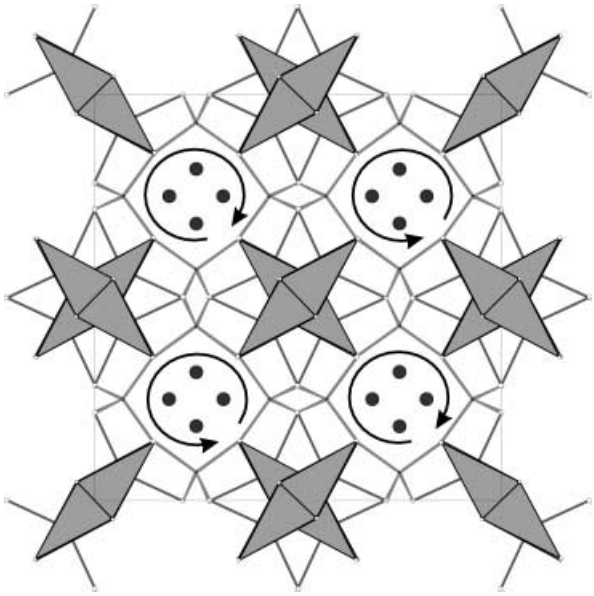

Figure 1. View of the unit cell down *c* (gray prisms containing the Nb atoms in eightfold coordination, black dots: P, white dots: S; large dark gray dots: alkali metal atoms (disordered)); black circles with arrows indicate the helicity of the chains, adjacent helices have opposite sense of rotation.

tances ranging between 2.499(5) and 2.617(5) Å). The S–S lengths of 2.022(10) Å and 2.025(10) are compatible with the presence of disulfide groups. The P–S lengths of 2.025(5)–2.061(6) Å are unexceptional. The Nb–Nb length through the shared rectangular face varies from 3.117(2) Å for $CsNb_2P_2S_{12}$ and 3.107(2) Å for $RbNb_2P_2S_{12}$ to 3.087(1) Å for $KNb_2P_2S_{12}$. It is thus slightly longer than the Nb–Nb lengths for Nb^{IV} chalcogenides such as $Rb_2Nb_2P_2S_{11}$,[15] ANb_2PS_{10}, (A = Na, Ag)[16] $Nb_2Y_2X_6$ (Y = S, Se; X = Br, I) (2.832–2.932 Å),[17] or Nb_2Te_6I (2.834 Å),[18] slightly shorter than those in Nb^{V} chalcogenides such as $NbTe_4I$ (3.362 Å),[19] and comparable to the Nb–Nb lengths in the mixed-valence compounds $(NbQ_4)_nI$[20] and $Nb_4OTe_9I_4$.[21] The increase in the Nb–Nb separations may be related to the size requirement of the alkali metal ions in the framework channels. These $[Nb_2S_{12}]$ and $[PS_4]$ units are linked in an alternating fashion, as indicated in Figure 1, into helical strands spiraling around the fourfold screw axes of the unit cell. Each $[PS_4]$ group links two $[Nb_2S_{12}]$ units and acts as a bischelating ligand.

Helix formation and framework channels: Figure 2a shows a biprism unit coordinated by four PS_4^{3-} ions, where one S atom of each $[PS_4]$ group is located at the edge atoms of the biprism and a second S atom caps its rectangular face. Because of their tetrahedral symmetry the two capping $[PS_4]$ groups may have different (up/down) orientation with respect to the biprism (see Figure 2b); the chelating nature of

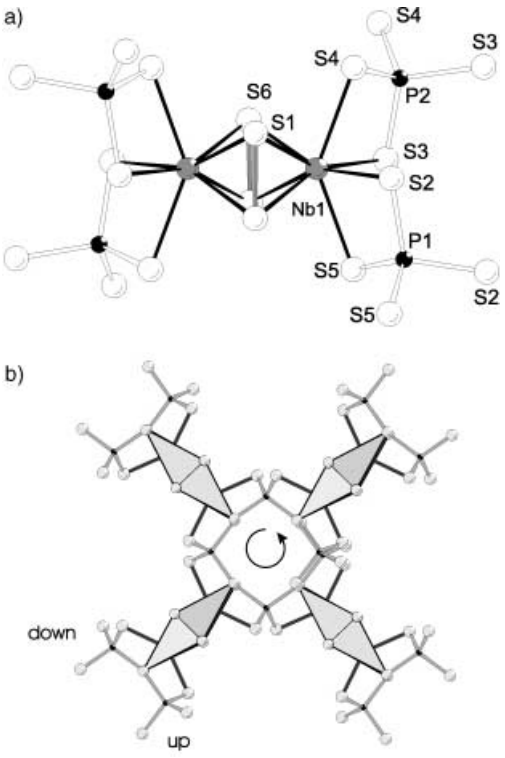

Figure 2. a) The basic building blocks of the $CsNb_2P_2S_{12}$ structure: $[Nb_2S_{12}]$ units connected by means of $[PS_4]$ tetrahedra. The S atoms of each $[PS_4]$ group occupy one edge and one capping position of adjacent bipyramidal $[Nb_2S_{12}]$ units. The Nb–Nb length with the $[Nb_2S_{12}]$ units of $CsNb_2P_2S_{12}$ is 3.117(2) Å, the S–S separations across the shared face are 2.022(10) Å and 2.025(10) Å. b) Repeat unit of a helix containing four $[Nb_2S_{12}]$ units interconnected by thiophosphate groups. The D_2 symmetry of the individual units leads to the formation of a helix chain.

the $[PS_4]$ ligand leads to an idealized D_2 or C_{2h} symmetry of the $[Nb_2(S_2)_2(PS_4)_4]$ units with two adjacent or opposite $[PS_4]$ groups pointing "up" and "down". In the structure of the title compound the $[Nb_2(S_2)_2(PS_4)_4]$ units have idealized D_2 symmetry, that is, the upper corner of each biprismatic unit is connected to the lower corner of an adjacent unit. This type of connectivity leads to the formation of a helical chain with four biprismatic units per repeat distance about the fourfold axes parallel *c* and a pitch angle of approximately 90°, as illustrated in Figures 2b.

The "prism helix" in the structure of $CsNb_2P_2S_{12}$ may be either left- or right-handed. The spiral chains around adjacent axes, which are cross-linked by common $[PS_4]$ groups, have opposing senses of rotation as indicated by the arrows in Figure 1. Adjacent helices with the same sense of rotation are not interconnected by common units. The $[NbPS_6]$ portion of the structure is quasi-one-dimensional: it is an inorganic double helix that is built up from non-interacting interpenetrating spiral $[NbPS_6]$ chains. This structural arrangement leaves large channels which are occupied by the Cs^+ cations. The cations are surrounded by eight S neighbors at distances between 3.1 and 4.0 Å.

The helix formation as well as the cross-linking of the helices are illustrated in Figure 1 and 2b. Four $[Nb_2S_{12}]$ and $[PS_4]$ units centered about the fourfold inversion axes form a set of large tunnels with a diameter of approximately 5 Å (coordinate to coordinate) that contain the metal cations. The cation sizes (K^+: 1.39 Å, Rb^+: 1.51 Å, Cs^+: 1.71 Å)[22] are small compared to the diameter of the large tunnel. The cations can therefore "rattle" within the channels as indicated by their disorder and their large and anisotropic displacement parameters. The large tunnel diameter, the high displacement parameters for the A^+ cations inside the tunnel, the synthesis of the isostructural series $ANb_2P_2S_{12}$, as well as the fractional distribution of the A^+ ions over several lattice sites indicate that $ANb_2P_2S_{12}$ (A = alkali metal) may be suitable hosts for ion-exchange reactions.

Physical properties and electronic structure:

Vibrational and spectral properties: According to the results of the X-ray structure determination the spectroscopically relevant units are the $[Nb_2S_{12}]$ cage and the $[PS_4]$ groups. The IR spectrum of $CsNb_2P_2S_{12}$ that is presented in Figure 3 shows strong absorptions at 674, 630, 583, 550, and 307 cm^{-1} and weak bands/shoulders at 527, 457, 353, 275, 255, 245, 220, and 207 cm^{-1}. In analogy to $TaPS_6(Se)$[14] or $Nb_4P_2S_{21}$[23] the absorbance at 583 cm^{-1} may be assigned to a S–S stretching vibration of the pyramidal $[Nb_2S_{12}]$ units, and the intense bands at 550 cm^{-1} and 307 cm^{-1} are attributed to PS_4[24] and Nb-$(S_2)_2$ P–S stretching modes, while the high frequency bands at 674 and 630 cm^{-1} may be either PS_4 stretching modes or combination bands (307 + 353 cm^{-1}, 353 + 275 cm^{-1}). Deformation modes of the $[PS_4]$ groups may contribute to the set of bands observed in the region between 400 and 220 cm^{-1}. Absorbances in a related spectral range were observed for metal thiophosphates such as NbP_2S_8[23] or $CrP_3S_{9.25}$.[25]

No meaningful diffuse reflectance spectrum of $CsNb_2P_2S_{12}$ could be obtained. Based on Drude's model this could be

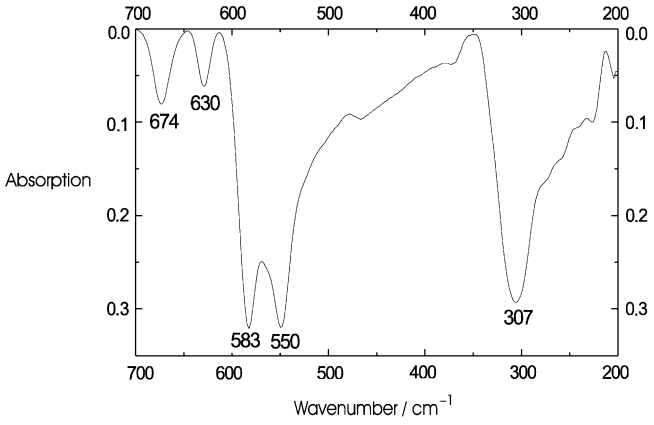

Figure 3. IR spectrum of $CsNb_2P_2S_{12}$.

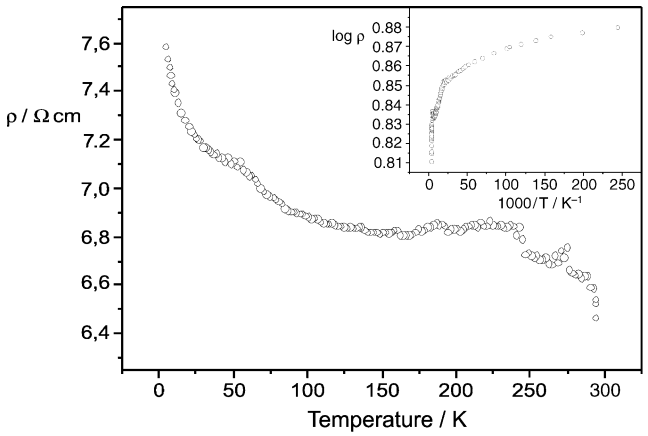

Figure 5. Plot of logρ verus $1/T$ for $CsNb_2P_2S_{12}$. The energy gap from the linear part in the logρ versus $1/T$ plot is 0.07 eV.

compatible with metallic properties.[26] The computed density of states (DOS) based on the results of ab initio LMTO-ASA band structure calculations[27,28] (spin-polarized) that shows that the Fermi level (E_F) is located in a local DOS minimum but with a significant DOS at E_F (Figure 4). Based on a formal charge balancing according to $(A^+)(Nb^{4.5+})_2(S_2^{2-})_2(PS_4^{3-})_2$, $ANb_2P_2S_{12}$ is mixed-valent. The Nb atoms are in bicapped trigonal-prismatic coordination; this results

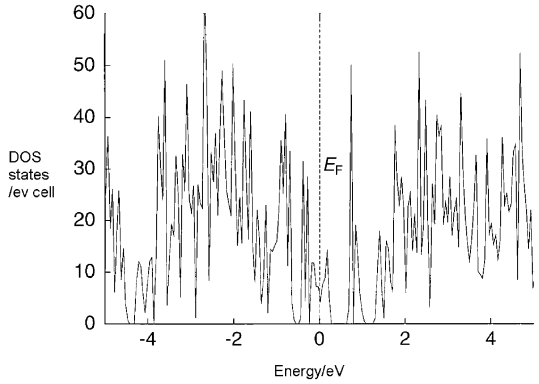

Figure 4. Total LMTO-ASA density of states for $CsNb_2P_2S_{12}$. The vertical line marks the Fermi energy.

in a one below four crystal field splitting of the Nb 4d orbital set. The HOMO of the $[Nb_2S_{12}]$ unit, which is the in-phase combination of the low lying Nb 4d(z^2) orbitals (Nb–Nb vector $\equiv$ z axis of the local coordinate system) is singly occupied and strongly metal–metal bonding. The narrow peak of width 0.7 eV in the computed density of states at the Fermi level corresponds to these Nb–Nb bonding states within the $[Nb_2S_{12}]$ unit.

Electrical transport properties: We have measured the resistivity versus temperature of a $KNb_2P_2S_{12}$ powder sample (which could be most easily contacted) by a standard four-probe technique. The room-temperature value of the specific resistivity $\rho_b \approx 6.47\ \Omega$cm indicates that $KNb_2P_2S_{12}$ may be considered a narrow gap semiconductor. A plot of logρ versus $1/T$ (Figure 5) shows slightly nonlinear behavior in the high-temperature regime; on the other hand, a variation of logρ versus $1/T^{1/2}$ shows almost linear behavior in this temperature range. This would be expected from variable range hopping conduction in 1D systems.[29] The data therefore suggest that thermally-activated conduction across a gap is insufficient for understanding the electrical properties of $KNb_2P_2S_{12}$.

Magnetic properties: If $CsNb_2P_2S_{12}$ were a simple metal, Pauli paramagnetism of the conduction electrons would be expected. Alternatively, an insulating phase would show simple Curie–Weiss-type behavior. The magnetic susceptibility data from measurements obtained with a vibrating sample magnetometer on a $\approx$65 mg powder sample, which was prepared by manually grinding selected single crystals, are shown in Figure 6. These values have been corrected for the container as well as for ion core diamagnetism (-187×10^{-6} emu mol^{-1}).[30] The data can be fitted by using an expression of the form $\chi = C/(T-\theta)+\chi_0$ with $C = 7.98(2)\times10^{-3}$ emu mol^{-1}, $\theta = 1(1)$ K, and a temperature-independent contribution $\chi_0 = 2.34(2)\times10^{-4}$ emu mol^{-1}. The computed

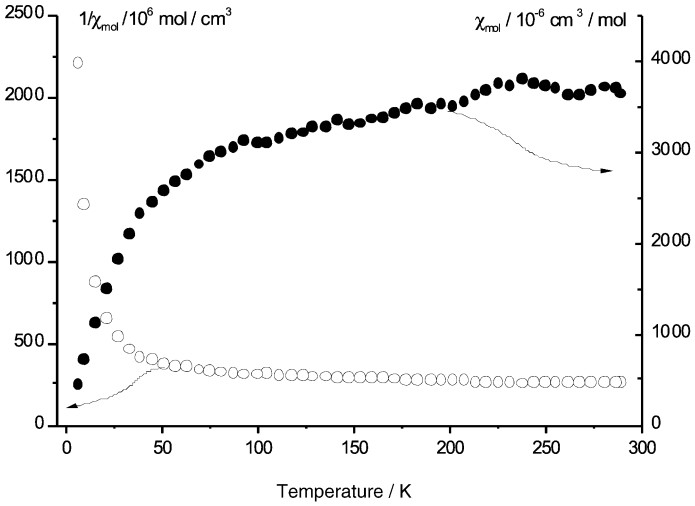

Figure 6. Temperature dependence of the magnetic susceptibility (left) and inverse magnetic susceptibility (right) of $CsNb_2P_2S_{12}$. The data have been corrected for core diamagnetism.

magnetic moment at room temperature is 0.79 μ_B. The large χ_0 value indicates a significant degree of Pauli paramagnetism; comparable values have been reported for Zintl phases such as K_8In_{11}.[31] The Curie tail at low temperature is a common feature which is usually attributed to small amounts of paramagnetic or ferromagnetic impurities. Measurements at different fields, however, show the absence of ferromagnetic impurities; furthermore, the sample was single phase based on X-ray powder diffractometer data, and niobium chalcogenides (which could be possible impurities) are known to be either diamagnetic or metallic.

ESR and ^{31}P NMR spectroscopy: To obtain a more reliable picture of the electronic properties, EPR measurements were performed on a $CsNb_2P_2S_{12}$ powder sample. The ESR spectrum in Figure 7 shows one broad signal with Lorentzian shape. Its isotropic g value of 1.992 and the width of 40×10^{-3} T (400 G) are typical for a metal with delocalized conduction electrons. Narrow resonance peaks with a width of approximately 10 G have been found in 1D organic conductors.[32] Figure 8a shows the ^{31}P-MAS-NMR spectrum at room temperature; the two signals at $\delta = 123.7$ and 145.9 ppm are assigned to the two crystallographically independent phosphorus atoms of the [PS_4] groups. The signals are shifted by approximately 60–80 ppm with respect to those in diamagnetic compounds such as $LiTi_2(PS_4)_3$ ($\delta =$ 64.1 ppm).[33]

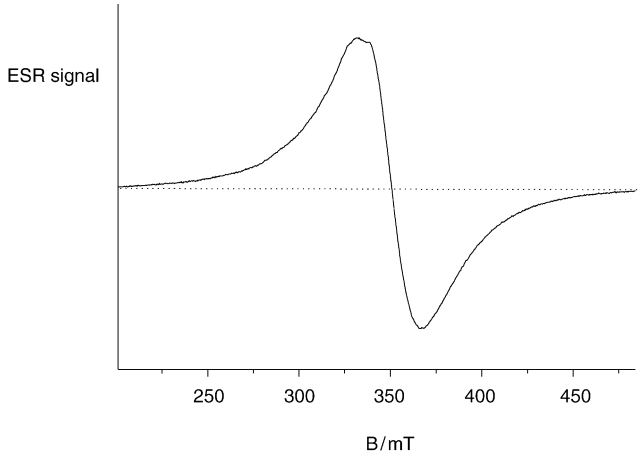

Figure 7. ESR powder spectrum of $CsNb_2P_2S_{12}$ ($T = 298$ K).

Figure 9 shows the temperature dependence of the ^{31}P shifts. Contrary to the situation in a metallic compound, the ^{31}P resonance shift is seen to be temperature dependent; however, this temperature dependence is opposite to the typical Curie-type behavior expected for a compound with localized unpaired electrons. Rather, the linear increase of δ observed for both phosphorus sites (T-coefficients near 0.1 ppm K^{-1}) suggests that the density of states at the Fermi level increases with increasing temperature. This result is pleasingly consistent with the thermally activated electrical transport behavior and further supported by the electronic structure calculations below.

Likewise, the chemical shift observed for the ^{133}Cs NMR signal lies outside of the typical range usually observed for ^{133}Cs in diamagnetic compounds. Again, the δ_{iso} value of 621 ppm versus 1 M aqueous CsCl solution is attributed to the effect of delocalized unpaired electron spin density at the Cs sites. The spectrum shown in Figure 8b also reveals numerous MAS spinning side bands, reflecting the effect of MAS on the quadrupolar satellite transitions.

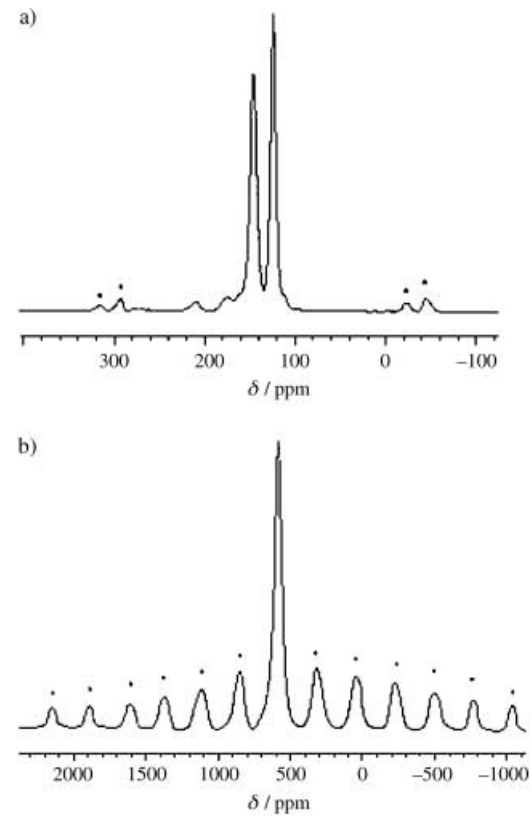

Figure 8. a) ^{31}P MAS-NMR spectrum of $CsNb_2P_2S_{12}$ at room temperature. b) 26.3 MHz ^{133}Cs MAS-NMR spectrum of $CsNb_2P_2S_{12}$ at 298 K. Spinning sidebands are indicated by asterisks.

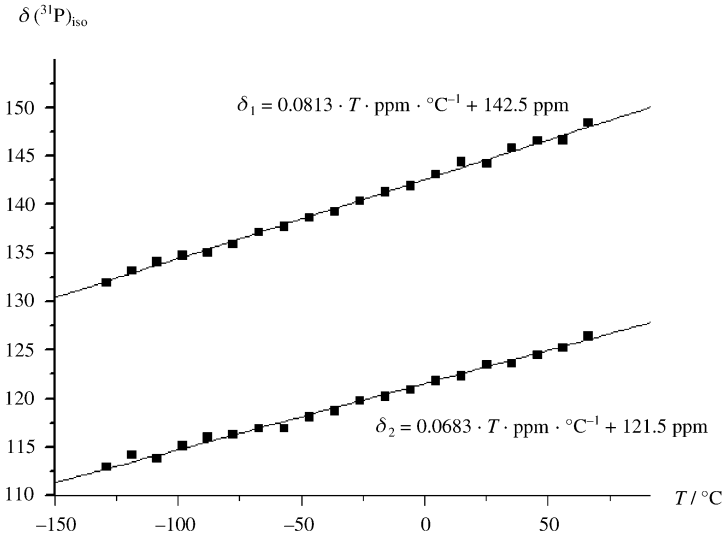

Figure 9. Temperature dependence of the ^{31}P chemical shifts in $CsNb_2P_2S_{12}$.

Band electronic structure: The electronic structure of $ANb_2P_2S_{12}$ can easily be understood in terms of its building blocks, $[Nb_2(S_2)_2(S^{2-})_8]$ units and $[PS_4]$ connector groups. According to the formal description $(A^+)(Nb^{4.5+})_2(S_2^{2-})_2(PS_4^{3-})_2$, each $[Nb_2S_{12}]$ unit carries one electron, so that each niobium center is in the oxidation state $Nb^{4.5+}$ ($d^{0.5}$). In bicapped trigonal-prismatic coordination there is a one below four crystal field splitting of the Nb 4d orbital set. The HOMO of the $[Nb_2S_{12}]$ unit, which is the in-phase combination of the low-lying Nb $4dz^2$ is singly occupied and metal–metal bonding. The computed DOS based on tight-binding calculations within the extended Hückel framework reproduce all features of the LMTO-ASA-DOS provided in Figure 4. This indicates that the electronic state of affairs is represented well by the EH method. Figure 10 shows the bottom four d-block bands of the $[Nb_2P_2S_{12}]^-$ framework. These bands are largely represented by the bottom d-block orbitals of each $[Nb_2S_{12}]$ unit shown in Scheme 1. They are

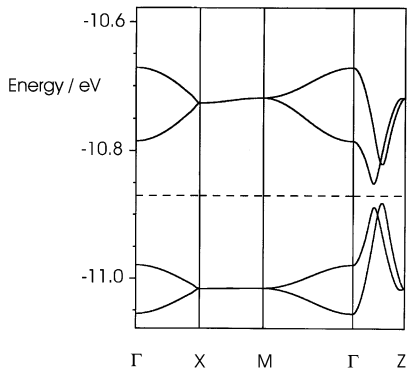

Figure 10. Dispersion relations for the bottom portion of the 4d block bands of the 3D-$NbPS_6$ lattice of $CsNb_2P_2S_{12}$. The horizontal bar refers to the Fermi level corresponding to $CsNb_2P_2S_{12}$. $\Gamma=(0,0,0)$, $X=(-a^*/2, b^*/2, 0)$, $M=(-a^*/2, b^*/2, 0)$, and $Z=(-a^*/2, b^*/2, 0)$.

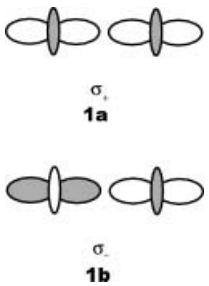

Scheme 1. The bottom d-block orbitals of each $[Nb_2S_{12}]$ unit. See text for details.

labeled σ_+ (1a) and σ_- (1b), where the subscripts + and − indicate that the d orbitals are combined in phase and out of phase, respectively. Only the metal d block orbitals are shown for simplicity. The primitive cell contains eight Nb atoms, that is, there are four Nb_2S_{12} units per unit cell. The four bands at Γ represent the four possible combinations of the σ_+ bands of the four $[Nb_2S_{12}]$ units. The Fermi level, marked by the dashed horizontal bar in Figure 10 separates the two lower, occupied bands from the two higher, unoccupied ones. This picture indicates that the compounds $ANb_2P_2S_{12}$ may be considered narrow gap (indirect) semiconductors, the computed band gap of approximately 0.05 eV being in the range of kT at room temperature ($\approx$0.04 eV). These findings support a picture of thermally-activated hopping conductivity, which could explain the electrical transport behavior of $CsNb_2P_2S_{12}$ and the ^{31}P chemical shift temperature dependence. Along Γ-X-M, perpendicular to the helix direction, the σ bands are flat (the tetragonal symmetry of the cell leads to the degeneracy along X-M). This is expected because the interactions between the individual chains are supposed to be weak. Along the helix chain, the σ bands develop a slightly higher dispersion, although the interaction with $[PS_4]$ groups does not provide the possibility of strong interactions between the $[Nb_2S_{12}]$ units. The crucial features are two avoided crossings along Γ-Z that lead to the formation of a small band gap. The lower two bands are symmetric and antisymmetric with respect to the fourfold inversion axis, the upper two bands have the same symmetry. The small gap is not therefore caused by factors such as electron–electron interactions, it is a sole consequence of the structure symmetry.

Conclusion

We have prepared by "alkali metal intercalation" a new group of niobium thiophosphates whose structure contains helical double chains. They exhibit activated electrical transport behavior and may be considered chalcogenide analogues of the well-known phosphate bronzes. They are the first quasi-metallic transition metal thiophosphates reported and may open a synthetic entry to a new class of low-dimensional materials with interesting properties. The synthesis of the title compounds with cations located inside the framework pores suggest several areas of additional research. i) These compounds may be derivatized by "soft chemistry" methods such as ion exchange. ii) The topotactic oxidation or reduction of these compounds may lead to new low-dimensional niobium chalcogenides with metallic properties along the helical niobium thiophosphate strands. iii) It is worthwhile to pursue the matter of ionic mobility within the channels.

Experimental Section

Materials: Starting materials were niobium metal powder (H.C. Starck, 99.999% purity), potassium (Merck, 99.9% purity), P_2S_5 (Fluka, 99.99% purity), $K_2S/Rb_2S/Cs_2S$, and S powder (Riedel, 99.999%). All starting compounds and products were examined by X-ray powder diffraction, using a Siemens D5000 diffractometer with a $Cu_{K\alpha}$ source.

Alkali metal Sulfide, A_2S: The alkali metal sulfides K_2S, Rb_2S, and Cs_2S were made following a modified procedure described in reference [32]: Alkali metal (10 g) was placed under an argon atmosphere on the glass frit of a Schlenk tube. The tube was cooled to −78 °C using a dry ice/acetone bath and NH_3 (approximately 30 mL) was condensed into the tube. After the metal was dissolved, elemental sulfur (1.6 g) was placed on the frit and dissolved by condensing a second portion of NH_3 onto the reactants. The resulting dark blue solution was stirred and NH_3 was allowed

to evaporate. A third portion of NH_3 was condensed onto the product to ensure that the reaction was complete. After evaporating the NH_3 a light yellow product was obtained. The yellow color indicates contamination with A_2S_2 (pure A_2S should be white). Samples with a stronger yellow tone must be subjected to an additional reduction with the corresponding alkali metal. All substances were handled under an argon atmosphere in a stainless steel glove box.

Preparation of $CsNb_2P_2S_{12}$: Nb (0.186 g, 2 mmol), P_2S_5 (0.222 g, 1 mmol), Cs_2S (0.149 g, 0.5 mmol), and S (0.208 g, 6.5 mmol) were sealed under vacuum ($<10^{-5}$ bar) in a silica tube and placed in a programmable chamber furnace. The sample was heated up to 600 °C. After five days the sample was cooled to room temperature at a rate of 1 °C min^{-1}. The yield of the metallic black crystalline material was quantitative based on the initial metal content as shown by X-ray powder diffraction. A semiquantitative microprobe analysis (EDAX) indicated the presence of Cs, Nb, P and S in an approximate atomic ratio of 1:2:2:12. Differential scanning calorimetry (DSC) measurements indicate that $CsNb_2P_2S_{12}$ melts congruently at 402 °C and has a glass transition at 254 °C.

Preparation of $RbNb_2P_2S_{12}$: Nb (0.186 g, 2 mmol), P_2S_5 (0.222 g, 1 mmol), Rb_2S (0.101 g, 0.5 mmol), and S (0.208 g, 6.5 mmol) were sealed under vacuum ($<10^{-5}$ bar) in a silica tube and placed in a programmable chamber furnace. The sample was heated up to 700 °C. After five days the sample was cooled down to room temperature at a rate of 1 °C min^{-1}. A semiquantitative EDAX analysis indicated to presence of Rb, Nb, P and S in an approximate atomic ratio of 1:2:2:12.

Preparation of $KNb_2P_2S_{12}$: Nb (0.186 g, 2 mmol), P_2S_5 (0.222 g, 1 mmol), K_2S (0.055 g, 0.5 mmol), and S (0.208 g, 6.5 mmol) were sealed under vacuum ($<10^{-5}$ bar) in a silica tube and placed in a programmable chamber furnace. The sample was heated up to 700 °C. After five days the sample was cooled down to room temperature at a rate of 1 °C min^{-1}. A semiquantitative EDAX analysis indicated the presence of K, Nb, P and S in an approximate atomic ratio of 1:2:2:12.

Structure determination: The structures of $CsNb_2P_2S_{12}$, $RbNb_2P_2S_{12}$, and $KNb_2P_2S_{12}$ were determined from single crystal X-ray diffraction data. The crystals were mounted on a glass fiber with epoxy, and intensity data were collected on a Nicolet P2$_1$ ($CsNb_2P_2S_{12}$) or a Siemens P4 ($RbNb_2P_2S_{12}$, $KNb_2P_2S_{12}$) automated four-circle diffractometer equipped with a monochromated $Mo_{K\alpha}$ source ($\lambda = 0.71073$ Å), a graphite monochromator, and a scintillation counter. 25 reflections found during the initial search in the range $2\theta = 4$–15° could be indexed with tetragonal unit cells, the final unit cell dimensions and their standard deviations were determined from least-squares fits of the setting angles of 25 reflections in the range $10 \le 2\theta \le 25°$. The final results are compiled in Table 1.

Data collections were performed with a θ–2θ scan mode on four octants $4 \le 2\theta \le 54°$. Three standard reflections from diverse regions of reciprocal space, which were monitored every 97 scans, indicated stable experimental conditions during the data collection. The systematic absence conditions (*hkl*, $h + h + l = 2n$; *h0l*, $h + k = 2n$; *0kl*, $k + l = 2n$) were characteristic of the tetragonal space group $I\bar{4}2d$ (no. 122), and the refinement results proved this choice to be correct.

Table 1. Crystal data and structure refinement for $CsNb_2P_2S_{12}$.

empirical formula	$CsNb_2P_2S_{12}$	$RbNb_2P_2S_{12}$	$KNb_2P_2S_{12}$
formula weight	765.39	717.95	671.58
diffractometer	Siemens P4	Siemens P4	Siemens P4
λ [Å]	0.71073	0.71073	0.71073
monochromator	graphite	graphite	graphite
data collection mode	ω-scan	ω-scan	ω-scan
crystal size [mm]	$0.1 \times 0.1 \times 0.1$	$0.1 \times 0.1 \times 0.1$	$0.1 \times 0.1 \times 0.1$
T [K]	293	201	201
crystal system	tetragonal	tetragonal	tetragonal
space group	$I\bar{4}2d$ (No. 122)	$I\bar{4}2d$ (No. 122)	$I\bar{4}2d$ (No. 122)
a [Å]	15.923(2)	15.8881(15)	15.8525(9)
c [Å]	13.238(3)	13.1321(14)	13.1192(11)
V [Å^3]	3356.4(10)	3315.0(6)	3296.9(4)
Z	8	8	8
ρ_{calcd} [g cm^{-3}]	3.029	2.877	2.706
μ ($Mo_{K\alpha}$) [mm^{-1}]	7.738	5.976	3.328
θ range	2.00–26.99	2.56–26.98	2.01–27.00
data collected	1875	1877	2501
unique data	1032 ($R_{int} = 0.0457$)	1035 ($R_{int} = 0.0466$)	1202 ($R_{int} = 0.0235$)
index ranges	$0 \le h \le 16$, $0 \le k \le 20$, $0 \le l \le 16$	$-1 \le h \le 16$, $-1 \le k \le 20$, $-1 \le l \le 16$	$-1 \le h \le 20$, $-1 \le k \le 20$, $-1 \le l \le 16$
refinement method	full-matrix, based on F^2	full-matrix, based on F^2	full-matrix, based on F^2
parameters	83	83	83
final R indices [$I > 2\sigma(I)$]			
$R1$	0.0499	0.0472	0.0241
$wR2$	0.1169	0.0755	0.0576
R indices (all data)[a,b]			
R	0.0774	0.0925	0.0366
WR	0.1260	0.0850	0.0647
goodness-of-fit on F^2	0.895	1.050	1.055
extinction coefficient	0.00000(7)	0.00020(3)	0.00056(5)
largest diff. peak and hole [e Å^{-3}]	1.569 and −1.445	0.69 and −0.72	0.66 and −0.69

[a] $R(|F|) = (\Sigma||F_o| - |F_c||)/\Sigma|F_o|$. [b] $wR(F^2) w = \{\Sigma w(|F_o^2| - |F_c^2|)^2/\Sigma wF_o^2\}^{1/2}$, $w = [\sigma^2(F) + 0.0010\,F^2]^{-1}$.

Data reduction was done by applying Lorentz and polarization corrections. The processed data were corrected for absorption effects using the XEMP routines of the SHELXTL/PC[34] program package. Further details relevant to the data collection and structure refinement are given in Table 1and in ref. [36].

The structures were solved by using direct methods (SHELXS86[37]) which revealed the atomic positions for Cs (Rb, K), Nb, P, and S. The structures were refined in a straightforward manner using the SHELX97 program package.[38] The final refinements were carried out on F_O^2. Atomic scattering factors for spherical neutral free atoms were taken from standard sources and anomalous dispersion corrections were applied.[39] From the final refinement cycle the compositions of the crystal used are $CsNb_2P_2S_{12}$, $RbNb_2P_2S_{12}$, $KNb_2P_2S_{12}$. The suitability of the anisotropic displacement parameters for the various atoms in the structures and the results of the susceptibility measurements suggest a stoichiometric composition.

Residual difference electron densities of $+1.57/-1.44$ e$^-$ Å^{-3} ($+0.69/-0.72$ e$^-$ Å^{-3}, $+0.66/-0.49$ e$^-$ Å^{-3}) are around 2% of the height of the heaviest element Nb. Analyses of F_O^2 versus F_C^2 as a function of F_O^2, setting angles or Miller indices revealed no unusual trends. Calculations performed at an intermediate stage in which the relative positional occupancies were refined, revealed a disorder of the cation positions, which was treated by refining the cation split positions with tied U_{ij} values. There are, however, no indications for nonstoichiometry. The correct enantiomorphs were chosen based on the Flack parameter. The final atomic parameters and interatomic distances are listed in Tables 2 and 3. Tables with anisotropic displacement parameters and the observed and calculated structure factors are available as Supporting Information. The molecular graphics were produced with the Diamond plot program.[40] Further details of the crystal structure investigation are available upon request

Table 2. Atom coordinates [$\times 10^4$] and isotropic displacement parameters [$Å^2 \times 10^3$] of A $Nb_2P_2S_{12}$ (A = Cs, Rb, K). *U*(eq) is defined as one third of the trace of the orthogonalized matrix *U*(ij).

	x	*y*	*z*	*U*(eq)
$CsNb_2P_2S_{12}$				
Nb(1)	663(1)	720(1)	2499(2)	16(1)
P(1)	551(4)	1/4	1/8	17(1)
P(2)	5830(4)	1/4	1/8	16(1)
Cs(1)	3184(1)	1/4	1/8	47(1)
Cs(2)	1/4	3203(15)	3/8	47(1)
S(1)	474(3)	5424(3)	1274(3)	21(1)
S(2)	1302(3)	1481(3)	997(3)	24(1)
S(3)	1449(3)	1541(3)	3869(4)	28(1)
S(4)	2198(3)	134(3)	2489(4)	24(1)
S(5)	2850(3)	4877(3)	2523(4)	24(1)
S(6)	4560(3)	457(3)	1296(4)	21(1)
$RbNb_2P_2S_{12}$				
Nb(1)	682(1)	701(1)	2502(3)	11(3)
P(1)	622(4)	1/4	1/8	12(2)
P(2)	5764(4)	1/4	1/8	17(2)
Rb(1)	3179(3)	1/4	1/8	43(1)
Rb(2)	1/4	3188(9)	3/8	43(1)
S(1)	476(3)	5428(4)	1289(5)	17(2)
S(2)	1395(4)	1486(4)	1030(4)	21(2)
S(3)	1462(3)	1471(4)	3920(5)	23(2)
S(4)	2161(4)	54(2)	2498(5)	16(1)
S(5)	2818(5)	4932(3)	2515(5)	21(2)
S(6)	4552(3)	458(4)	1296(4)	12(1)
$KNb_2P_2S_{12}$				
Nb(1)	689(1)	688(1)	2499(1)	13(1)
P(1)	698(2)	1/4	1/8	16(1)
P(2)	5694(2)	1/4	1/8	16(1)
K(1)	3171(3)	1/4	1/8	63(1)
K(2)	1/4	3179(7)	3/8	63(1)
S(1)	454(1)	5440(2)	1298(2)	18(1)
S(2)	1446(1)	1480(2)	1056(3)	23(1)
S(3)	1463(2)	1437(2)	3951(3)	20(1)
S(4)	2164(2)	−7(1)	2506(2)	20(1)
S(5)	2820(2)	4989(1)	2514(2)	21(1)
S(6)	4540(1)	455(2)	1301(2)	16(1)

from the Fachinformationszentrum Karlsruhe, 76344 Eggenstein-Leopoldshafen (fax: (+49) 7247-808-666; e-mail: crysdata@fiz-karlsruhe.de), on quoting the depository numbers CSD-412198 ($CsNb_2P_2S_{12}$), CSD-412199 ($RbNb_2P_2S_{12}$), and CSD-412200 ($KNb_2P_2S_{12}$).

Physical measurements:

Semiquantitative microprobe analysis: Semiquantitative Microprobe analysis was performed in a Zeiss DSM 962 scanning electron microscope equipped with a KEVEX energy dispersive spectroscopy detector. Data acquisition was performed with an accelerating voltage of 20 kV and a 1 min accumulation time.

FTIR spectra: FTIR spectra were recorded on solid samples in a CsI matrix. The samples were ground with dry CsI into a fine powder and pressed into transparent pellets. The spectra were recorded in the far-IR region (700–200 cm^{-1}, $\approx 5\ cm^{-1}$ resolution) with an FTIR spectrometer (2030 Galaxy-FT-IR, Mattson Instruments) equipped with a TGS/PE detector and a silicon beam splitter.

Optical spectroscopy: Optical diffuse reflectance measurements were made at room temperature with a Varian CARY5 double-beam, double-monochromator spectrophotometer operating in the 200–2000 nm region. The instrument was equipped with an integrating sphere and controlled by a personal computer. The measurement of diffuse reflectivity may be used to determine values for the optical band gap, which are in reasonable agreement with those obtained from single crystal absorption measurements. $BaSO_4$ was used as reference material (100% reflectivity assumed).[41]

Magnetic susceptibility measurements: Variable-temperature magnetic susceptibility data were collected for a 65 mg sample of $CsNb_2P_2S_{12}$ with a vibrating sample magnetometer (Foner-magnetometer, Princeton Applied Research), which was operated between 0.2 and 1 T. The instrument was calibrated with $Hg[Co(NCS)_4]$. Measurements at different field strengths confirmed that ferromagnetic impurities were absent. The diamagnetic correction was estimated from Pascal's constants to be $-180 \times 10^{-6}\ cm^3\,mol^{-1}$.[30]

Thermal analysis: Thermal analysis was performed on a Netzsch STA 429 Differential Thermal Analyzer. 20 mg of crystalline material were selected from the reaction product and ground to a fine powder. The sample was loaded into a small quartz tube with a flattened and polished bottom and sealed under vacuum. Heating and cooling rates were $2\,°C\,min^{-1}$. Sample integrity was checked by powder diffraction after each run.

Table 3. Selected bond lengths [Å] for $ANb_2P_2S_{12}$ (A = Cs, Rb, K).[a]

Bond	A =			Bond	A =		
Bond	K	Rb	Cs		K	Rb	Cs
Nb(1)–S(1)#2	2.499(5)	2.489(7)	2.496(3)	Nb(1)–Nb(1)#10	3.117(2)	3.1073(19)	3.087(1)
Nb(1)–S(6)#6	2.515(5)	2.516(6)	2.517(3)	S(1)–S(1)#1	2.025(10)	2.033(14)	2.003(6)
Nb(1)–S(6)#8	2.543(5)	2.538(6)	2.515(3)	S(6)–S(6)#13	2.022(10)	2.034(12)	2.052(6)
Nb(1)–S(2)	2.541(5)	2.564(7)	2.569(3)				
Nb(1)–S(1)#7	2.518(5)	2.520(6)	2.524(3)	A(1)–S(2)	3.424(6)	3.273(7)	3.187(5)
Nb(1)–S(3)	2.562(5)	2.551(7)	2.558(3)	A(1)–S(2)#2	3.424(6)	3.273(7)	3.187(5)
Nb(1)vS(5)#9	2.598(5)	2.638(7)	2.612(3)	A(1)–S(3)#5	3.551(5)	3.515(6)	3.503(3)
Nb(1)–S(4)	2.617(5)	2.565(6)	2.585(3)	A(1)–S(3)#18	3.551(5)	3.515(6)	3.503(3)
mean	2.549	2.548	2.547	A(1)–S(4)#15	3.558(5)	3.445(6)	3.360(5)
				A(1)–S(4)#17	3.558(5)	3.445(6)	3.360(5)
				A(1)–S(6)#2	3.922(5)	3.911(6)	3.902(5)
P(1)–S(5)#16	2.025(5)	2.021(7)	2.037(3)	A(1)–S(6)	3.922(5)	3.911(6)	3.902(5)
P(1)–S(5)#9	2.025(5)	2.021(7)	2.037(3)				
P(1)–S(2)	2.043(6)	2.046(6)	2.021(3)	A(2)–S(3)	3.13(2)	3.195(14)	3.23(1)
P(1)–S(2)#2	2.043(6)	2.046(6)	2.021(3)	A(2)–S(3)#18	3.13(2)	3.195(14)	3.23(1)
mean	2.034	2.034	2.029 K(2)–S(5)#18	A(2)–S(5)#18	3.17(2)	3.250(14)	
				A(2)–S(5)	3.17(2)	3.250(14)	3.34(1)
P(2)–S(3)#17	2.026(6)	2.008(6)	2.039(3)	A(2)–S(2)#12	3.569(6)	3.509(6)	3.498(4)
P(2)–S(3)#15	2.026(6)	2.008(6)	2.039(3)	A(2)–S(2)#2	3.569(6)	3.509(6)	3.498(4)
P(2)–S(4)#15	2.061(6)	2.066(7)	2.045(3)	A(2)–S(1)#9	3.921(13)	3.918(10)	3.92(1)
P(2)–S(4)#17	2.061(6)	2.066(7)	2.045(3)	A(2)–S(1)#19	3.921(13)	3.918(10)	3.92(1)
mean	2.044	2.037	2.042				

[a] Symmetry transformations: #1: $-x, -y+1, z$; #2: $x, -y+1/2, -z+1/4$; #3: $-x, y+1/2, -z+1/4$; #4: $-y+1/2, x+1/2, -z+1/2$; #5: $-x+1/2, -y+1/2, z-1/2$; #6: $-y+0, -x+1/2, z+1/4$; #7: $y, x-1/2, z+1/4$; #8: $-x, y-1/2, -z+1/4$; #9: $y-1/2, -x+1/2, -z+1/2$; #10: $-x, -y, z$; #11: $-y+1/2, x-1/2, -z+1/2$; #12: $-x+1/2, -y+1/2, z+1/2$; #13: $-x+1, -y, z$; #14: $-y+1/2, -x, z-1/4$; #15: $y+1/2, x, z-1/4$; #16: $y-1/2, x, z-1/4$; #17: $y+1/2, -x+1/2, -z+1/2$; #18: $-x+1/2, y, -z+3/4$; #19: $-y+1, -x+1/2, z+1/4$.

NMR Studies: Nuclear magnetic resonance studies were carried out at 121.49 MHz using a Bruker CXP-300 spectrometer equipped with a magic-angle spanning probe from DOTY Scientific. Samples were spun within sapphire or zirconia spinners of 4 mm o.d. at speeds varying from 3.5 to 13.5 kHz. To avoid possible hydrolysis by atmospheric moisture, the spinners were sealed with a thin layer of high-vacuum grease and spun with evaporated liquid nitrogen. Typical 90° pulse length and relaxation delay were 5 μs and 4 min, respectively. ^{31}P chemical shifts are externally referenced to 85 % H_3PO_4 (downfield shifts positive). Temperature-dependent measurements were calibrated with a solid sample of lead nitrate. ^{133}Cs NMR spectra were obtained at 26.3 MHz, using a modified Bruker CXP-200 spectrometer equipped with a 7 mm multinuclear probe. Signals were acquired with 90° pulses, 5 min recycle delays at an MAS rotor frequency of 7.0 kHz.

ESR studies: X-band ESR measurements were made with a Bruker X-band EPR spectrometer with 100 kHz field modulation and the magnetic field was calibrated with DPPH (2,2-diphenyl-1-picrylhydrazyl; $g = 2.0036$) as an external standard.

Band structure calculations: Band structure calculations based on the structural parameters given in Table 1 were performed at the extended Hückel[42] and the LMTO-ASA[27,28] level in the tight-binding approximation. The EH calculations were carried out with the EHMACC software[43] and the following parameters: Nb, 5 s: $H_{ii} = -10.10$ eV, $\zeta = 1.89$; 5p: $H_{ii} = -6.86$ eV, $\zeta = 1.85$; 4d: $H_{ii} = -12.1$ eV, $\zeta_1 = 4.060$, $c_1 = 0.6401$, $\zeta_2 = 1.64$, $c_2 = 0.55516$. P, 3 s: $H_{ii} = -18.6$ eV, $\zeta = 1.75$; 3p: $H_{ii} = -14.0$ eV, $\zeta = 1.30$. S, 3 s: $H_{ii} = -20.0$ eV, $\zeta = 2.12$; 3p: $H_{ii} = -13.3$ eV, $\zeta = 1.83$. A detailed description of the LMTO-ASA method, including its application to the electronic structure of compounds, has been given elsewhere.[44] We give only a few details of the calculations here. The scalar relativistic Kohn–Sham–Schroedinger equation was solved, taking all relativistic effects into account, except for spin-orbit coupling. All k space integrations were performed using the tetrahedron method using 250 irreducible k points in the monoclinic Brillouin zone (BZ). The basis set consists of s, p and d orbitals for Cs and Nb, and s and p orbitals for P and S. The d orbitals of P and S were included in the tails of the LMTOs according to the Löwdin down-folding technique.[27] Since the present structures are rather open, special care was taken in filling the interatomic space. If only atom-centered spheres were used, the atomic sphere approximation (ASA) would lead to unsatisfactory results because of too large an overlap. It is therefore necessary to introduce interstitial spheres. The positions of the empty spheres were calculated by an automatic procedure developed by Krier et al.[28]

Acknowledgement

This work was supported by the Deutsche Forschungsgemeinschaft and the Fonds der Chemischen Industrie. We are indebted to Heraeus Quarzschmelze Hanau (Dr. Höfer) for a generous gift of silica tubes and to Sandra Stauf for the collection of the X-ray diffraction data.

[1] a) M. Greenblatt, *Chem. Rev.* **1988**, *88*, 31–55, and references therein; b) E. Canadell, M.-H. Whangbo, *Chem. Rev.* **1991**, *91*, 965–1034, and references therein.

[2] a) M. M. Borel, M. Goreaud, A. Frandin, Ph. Labbe, A. LeClaire, B. Raveau, *Eur. J. Solid State Inorg. Chem.* **1991**, *28*, 93–129, and references therein; b) M. Greenblatt, *Acc. Chem. Res.* **1996**, *29*, 219–228, and references therein.

[3] a) R. Buder, J. Devenyi, J. Dumas, J. Marcus, J. Mercier, C. Schlenker, H. Vincent, *J. Phys. Lett.* **1982**, *43*, L59-L63; b) C. Escribe-Filippini, K. Konate, J. Marcus, C. Schlenker, R. Almayrac, R. Aryloes, C. Rouceau, *Philos. Mag.* **1984**, *B50*, 321–330.

[4] C. Schlenker, J. Dumas, in *Crystal Chemistry and Properties of Materials with Quasi-One-Dimensional Structures*, (Ed.: J. Rouxel), Reidel: Dordrecht, The Netherlands, **1986**, pp. 135–177.

[5] J. A. Wilson, F. J. DiSalvo, S. Mahajan, *Adv. Phys.* **1975**, *24*, 117–200.

[6] R. H. Friend, A. D. Yoffe, *Adv. Phys.* **1987**, *36*, 1–94.

[7] a) A. Meerschaut, J. Rouxel, *J. Less-Common Met.* **1975**, *39*, 197–203; b) P. Monceau, N. P. Ong, A. M. Portis, A. Meerschaut, J. Rouxel, *Phys. Rev. Lett.* **1976**, *37*, 602–606.

[8] a) S. Furuseth, L. Brattas, A. Kjekshus, *Acta Chem. Scand.* **1975**, *29*, 623–631; b) S. Takahashi, T. Sambongi, *Solid State Commun.* **1984**, *49*, 1031–1034; c) C. Felser, E. W. Finckh, H. Kleinke, F. Rocker, W. Tremel, *J. Mater. Chem.* **1998**, *8*, 1787–1798; d) R. Seshadri, E. Suard, C. Felser, E. W. Finckh, A. Maignan, W. Tremel, *J. Mater. Chem.* **1998**, *8*, 2869–2874.

[9] J. K. Burdett, *Chemical Bonding in Solids*, Oxford University Press, New York, **1995**, chap. 5.

[10] a) R. Brec, *Solid State Ionics* **1986**, *22*, 3–30; b) M. Evain, R. Brec, M.-H. Whangbo, *J. Solid State Chem.* **1987**, *71*, 244–262; c) *Progress in Intercalation Research* (Eds.: W. Müller-Warmuth and R. Schöllhorn), Kluwer, **1995**, and references therein; d) G. Ouvrard, E. Prouzet, R. Brec, S. Benazeth, H. Dexpert, *J. Solid State Chem.* **1990**, *86*, 238–248; e) P. A. Joy, S. Vasudevan, *J. Am. Chem. Soc.* **1992**, *114*, 7792–7801; f) P. A. Joy, S. Vasudevan, *Chem. Mater.* **1993**, *5*, 1182–1191.

[11] R. Schöllhorn, *Angew. Chem. Adv. Mater.* **1988**, *100*, 1446–1454.; *Angew. Chem. Int. Ed. Engl. Adv. Mater.* **1988**, *27*, 1446–1454.

[12] S. Fiechter, W. F. Kuhs, R. Nitsche, *Acta Crystallogr.* **1980**, *36*, 2217–2220.

[13] M. Evain, M. Queignec, R. Brec, J. Rouxel, *J. Solid State Chem.* **1985**, *59-60 56*, 148–157.

[14] M. Evain, M. Queignec, R. Brec, C. Sourisseau, *J. Solid State Chem.* **1988**, *75*, 413–431.

[15] A. Gutzmann, W. Bensch, *Solid State Sci.* **2002**, *4*, 835–840.

[16] a) E. Y. Gohm S.-J. Kim, D. Jung, *J. Solid State Chem.* **2002**, *168*, 119–125; b) A. J. Woo, S.-J. Kim, Y. S. Park, E.-Y. Goh, *Chem. Mater.* **2002**, *14*, 518–523.

[17] H. F. Franzen, W. Hönle, H-G. v. Schnering, *Z. Anorg. Allg. Chem.* **1983**, *497*, 13–20.

[18] W. Tremel, *Inorg. Chem.* **1992**, *31*, 755–760.

[19] W. Tremel, *Chem. Ber.* **1993**, *126 125*, 2165–2170.

[20] J. Rouxel, *J. Solid State Chem.* **1986**, *61*, 305–321, and references therein.

[21] W. Tremel, *J. Chem. Soc. Chem. Commun.* **1992**, 709–710.

[22] R. D. Shannon, *Acta Crystallogr. Sect. A* **1976**, *32*, 751–767.

[23] M. Queignec, M. Evain, R. Brec, C. Sourisseau, *J. Solid State Chem.* **1986**, *63*, 89–109.

[24] H. Bürger, H. Falius, *Z. Anorg. Allg. Chem.* **1968**, *363*, 24–32.

[25] C. Sourisseau, P. Fragnaud, E. Prouzet, R. Brec, R. , *J. Solid State Chem.* **1994**, *112*, 299–306.

[26] S. Elliott, *The Physics and Chemistry of Solids*, Wiley, New York, **1998**, chap. 6.

[27] O. K. Andersen, *Phys. Rev. B* **1975**, *12*, 3060–3083; O. K. Andersen, O. Jepsen, *Phys. Rev. Lett.* **1984**, *53*, 2571–2574.

[28] G. Krier, O. Jepsen, A.Burkhardt, O. K. Andersen, *Program TB-LMTO-ASA 47 (tight binding-linear muffin tin orbital-atomic sphere approximation)*, Stuttgart, **1996**.

[29] N. W. Ashcroft, N. D. Mermin, *Solid State Physics*, Saunders, Philadelphia, **1976**, chap. 17.

[30] W. Haberditzl, Magnetochemie, Akademie Verlag, Berlin, **1968**, pp. 102–103.

[31] S. Sevov, J. E. Ostenson, J. D. Corbett, *J. Alloys Compd.* **1993**, *202*, 289–294.

[32] S. Kagoshima, H. Nagasawa, T. Sambongi, *One-Dimensional Conductors*, Springer, Berlin, **1988**.

[33] a) G. Regelsky, V. Derstroff, C. Gieck, W. Tremel, H. Eckert, unpublished results; b) G. Regelsky, Ph.D. Dissertation, Münster, **2000**.

[34] F. Feher, in *Handbuch der Präparativen Anorganischen Chemie* (Eds.: G. Brauer, Ferdinand Enke), Stuttgart, Germany, **1954**, pp. 280–281.

[35] SHELXTL/PC, G. M. Sheldrick, Siemens Analytical X-ray Instruments Inc., Madison, Wisconsin, USA.

[36] W. Tremel, M. Kriege, B. Krebs, G. Henkel, *Inorg. Chem.* **1988**, *27*, 3886–3895.

[37] G. M. Sheldrick, SHELXS-86, Program for Crystal Structure Solution, Universität Göttingen, Göttingen, **1986**.

[38] G. M. Sheldrick, SHELX97, Program for Crystal Structure Refinement, Universität Göttingen, Göttingen, **1997**.

[39] D. T. Cromer, J. T. Waber, *International Tables for X-Ray Crystallography*, Kynoch Press, Birmingham, England, **1974**, Vol. IV, Table 2.2A and Table 2.3.1.
[40] Diamond, *Visuelles Informationssystem für Kristallstrukturen*, K. Brandenburg, M. Berndt, G. Bergerhoff, Universität Bonn, **1998**.
[41] a) G. Kortüm, *Reflectance Spectroscopy*, Springer Verlag, New York, **1969**; b) R. J. H. Clarke, *J. Chem. Educ.* **1964**, *41*, 488 – 492; c) W. W. Wendlandt, H. G. Hecht, *Reflectance Spectroscopy* (Chemical Analysis, *Vol. 21*), Interscience, New York, **1966**.
[42] a) Extended Hückel approximation: R. Hoffmann, *J. Chem. Phys.* **1963**, *39*, 1397 – 1412; b) Weighted H_{ij} elements: J. H. Ammeter, H.-B. Bürgi, J. C. Thibeault, R. H. Hoffmann, *J. Am. Chem. Soc.* **1978**, *100*, 3686 – 3693; c) tight-binding approximation: M.-H. Whangbo, R. H. Hoffmann, *J. Am. Chem. Soc.* **1978**, *100*, 6093 – 6098; M.-H. Whangbo, R. H. Hoffmann, R. B. Woodward, *Proc. R. Soc. London Ser. A* **1979**, *366*, 23 – 46.
[43] EHMACC program for Extended Hückel Molecular and Crystal Calculations: M.-H. Whangbo, M. Evain, T. Hughbanks, M. Kertesz, S. Wijesekera, C. Wilker, C. Zheng, and R. Hoffmann.
[44] H. L. Skriver, *The LMTO Method*, Springer, Berlin, **1984**.

Received: August 22, 2001
Revised: July 8, 2003 [F3504]

